IJL, Issue 1, Vol. 23, 2024
https://doi.org/10.31900/ijl.v23i1.409

Research Article

IRAQI JOURNAL OF LASER

Refractive index biosensor based on offset technique of coreless fiber

Saraa J. Aldulimi*, Hanan J. Taher

Institute of Laser for Postgraduate Studies, University of Baghdad, Baghdad, Iraq
** Email address of the Corresponding Author: saraa.najm2101m@ilps.uobaghdad.edu.iq*

Article history: Received 27 Jul. 2023; Revised 5 Oct. 2023; Accepted 15 Oct. 2023; Published online15 Jun. 2024

Abstract: This paper suggested a biosensor structure using an offset technique between two similar coreless fiber (CF) segments spliced between two single-mode fibers (SMF) for refractive index (RI) measurement of the liquid pharmaceutical, where experimented with different lengths of CF sections for 10 mm, 15mm, 20 mm, and 25 mm with different offsets for 2.6 µm, 6.4 µm, and 18.3 µm of symmetric CF sections. This sensor tests different refractive indices (1, 1.333, 1.337, 1.369, 1.393) of liquid pharmaceuticals The wavelength shifting increases with decreasing length or displacement of offset. The highest sensitivity was achieved, 255.5 nm/RIU, with the smallest sensor size, corresponding to the highest refractive index of 1.393 for the Histadin syrup drug, obtained using the optimal length and offset. This sensor has the capability to detect various refractive indices of chemicals and biochemical liquids. Advantages of the proposed sensor include high sensitivity, adaptability, enabling faster real-time measurements, ease of manufacturing and operation, compact size, lightweight design, and low cost.

Keywords: Refractive index sensor, optical fiber biosensor, offset technique, coreless Fiber.

1. Introduction

Optical fiber biosensors (OFBS) are attracting an increasing number of researchers due to their advantages of high sensitivity and flexibility, enabling quicker and real-time measurements, ease of fabrication and operation, small size, lightweight, and low cost. This is because OFBS has a wide range of applications in the healthcare industry, including blood pressure monitoring, blood sugar monitoring, pharmaceutical dose control, drug identification, food control, and many other applications that require this type of sensor [1, 2].

Optical biosensors are technologies that track changes in light properties like refraction index, absorption, fluorescence, or light scattering brought on by the interaction that recognizes biological or chemical reaction processes by producing signals proportional to the concentration of an analytic in the reaction. Biological materials (such as enzymes, antibodies, antigens, receptors, nucleic acids, cells, and complete tissues) are analyzed using biosensors to assess the identity of illegal substances and to identify the formation of new pharmaceuticals [3-5]. Most optic fiber sensor structures achieve the principle work of Mach-Zehnder Interferometer MZI, which has been implemented using different fabrication techniques

such as optical fiber tapers [6, 7]. thin core fibers (TCF) [8], long-period grating cascade structures [9, 10] Photonic crystal fiber (PCF) [11], coreless fiber (CF)[12,13], and offset technique [14-16]. The offset structure of similar coreless fiber splits the light into two parts: one of them is the fundamental core mode propagating in the CF represented as core mode, and the other one is the drug sample represented as cladding modes; the different optical paths of the residual core mode and cladding modes could form an intermodal MZI [24]. The transmission spectrum of the interferometer is simply expressed as that of a two-mode interference:

$$I = I_{co} + I_{cl} + 2\sqrt{I_{co}\ I_{cl}\ \cos\emptyset} \quad (1)$$

Where I is the light intensity of the output light, Ico represents the intensities of the core, Icl defines as the cladding mode, and $\emptyset$ = is the phase difference of the two interference modes, which can be expressed as [25]:

$$\emptyset = \frac{2\pi(nco - ncl)L_{eff}}{\lambda} \quad (2)$$

Where nco represents the RIs of the optical fiber core, ncl is the effective cladding, L_{eff} represents the effective length of the two-mode interference paths, and λ is the wavelength in vacuum.

When $\emptyset = (2i + 1)\ \pi$, i is a positive integer, the interference dip appears, and the wavelength dip can be expressed as:

$$\lambda = \frac{2\pi(nco - ncl)Leff}{(2i + 1)\ \pi} \quad (3)$$

From Eq. 3, it can be seen that for the fixed interference path length, the position of the interference dip depends on the effective RI difference between the core and the cladding mode [26]. When the external environment RI changes, the effective RI of the cladding mode will change, while the effective RI of the fiber core mode will not change, which will lead to a change in the position of the wavelength dip [26], [25]. CF interacts with SMF to efficiently stimulate high-order cladding modes[17]. Meanwhile, CF can be used as a coupler in the sensor to split light and combine light. [18,19]. This work used the offset technique, compared to the other techniques, the offset technique has a simpler fabrication process with less complicated equipment.

In this study, was proposed a new structure has small size of the sensing region makes it easier to work with less susceptible to breakage, less consumption of coreless optical fiber when fabricating the structure, less waste of samples to be tested for their refractive index and lower cost compared to offset structure in previous studies. This structure achieved the highest sensitivity 255.5 nm/RIU, a smaller size due to using only 20 mm of sensing arm from CF segments. In the previous studies [20] proposed a single-mode fiber (SMF) sensor based on a core-offset inter-modal interferometer whose refractive index sensitivity was -64.889 nm/RIU in 2014 Jingli Fan et al [20]. In another study proposed a highly sensitive Mach-Zehnder interferometric refractive index sensor based on core-offset single-mode fiber the higher refractive index sensitivity of 78.7nm/RIU in 2015 Yong Zhao et al [21], while the proposed refractive index sensor based on the lateral offset of coreless silica interferometer achieved a higher refractive index sensitivity was 750 nm/RIU in 2018 Nur Faizzah et al. [22], and finally suggested S and U shape offset studying of the refractive index sensor based on coreless fiber higher sensitive was achieved in a novel S-shape equal 98.768 nm/RIU in 2022 Aya R. Mejble et al. [23].

This study showed the benefits of offset with similar sections of coreless fiber the sensitivity increasing when decreasing the length of coreless fiber sections. That achieved a smaller size of sensor device easy fabrication, easy to carry, low cost and it can link with accurate devices to be used in other applications. We used a structure for biosensor applications to detect the identity of liquid pharmaceutical droops and syrups, which, when increasing the refractive index, increases the wavelength shifting in a red direction.

2. Sensor Fabrication Process

The optical fiber sensing structure is shown in Figure 1, where d is the offset displacement, and L is the length of sensing regain. The single mode coreless-coreless single mode (SCCS) sensor structure comprises two segments of single-mode fiber (SMF) and two segments of coreless fiber CF in between. The four segments are spliced together. The schematic diagram of the (SCCS) sensor configuration is depicted in Figure 2 (a) the Left side for SMF input auto-splicing with CF, (b) the Right side for SMF input auto-splicing with CF, and (c) the offset splicing point of CF.

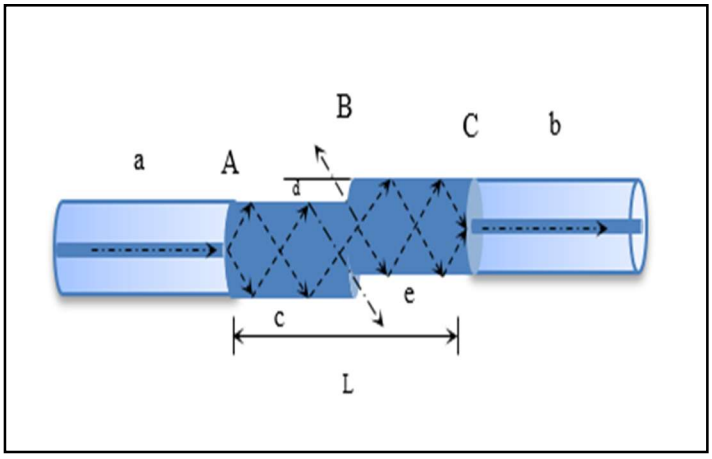

Fig.1. Schematic of sensing structure: A is the auto-splice point, B is the offset point, and C is the auto-splice point. c and e are similar sections of coreless fiber (CF). a, b are lead-in and lead-out of single-mode fibers (SMF).

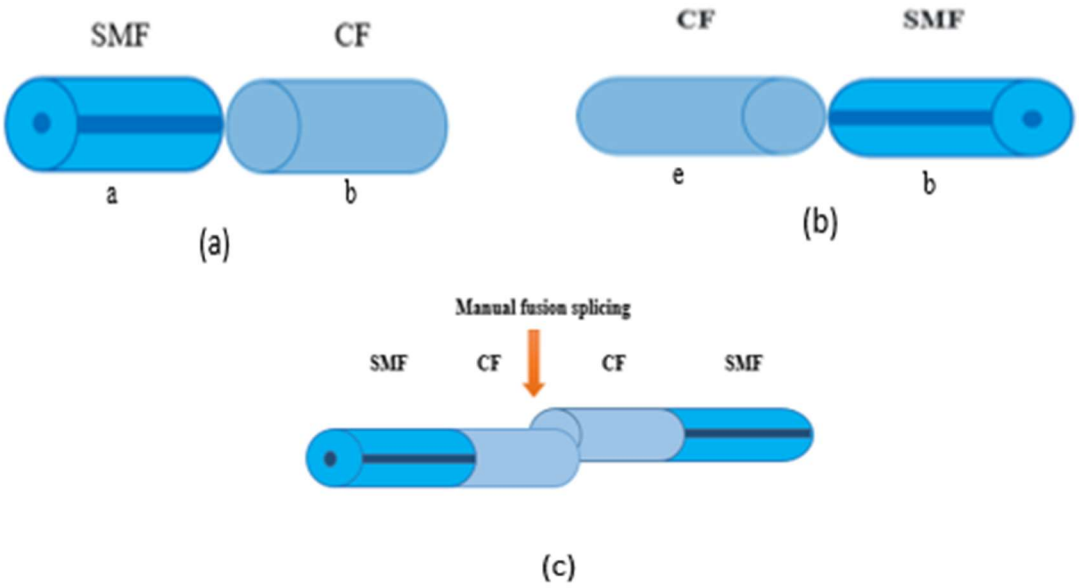

Fig.2: (a) Left side for SMF input auto splicing with CF, (b) Right side for SMF input auto splicing with CF and (c) Offset splicing point of CF.

The different offsets tested (2.6 µm, 6.4 µm, 12.1 µm, 18.3 µm), were tested by splicing each one of them with the different lengths of similar CF (10mm, 15 mm, 20mm, and 25mm). The offset point displacement was measured by microscope magnification 10X, and the length of CF was measured by a ruler. A microscope images for different offset distances (d) were shown in Figure 3 (a) d= 2.6 µm, (b) d= 6.4 µm, (c) d= 12.1 µm, and (d) d= 18.3.

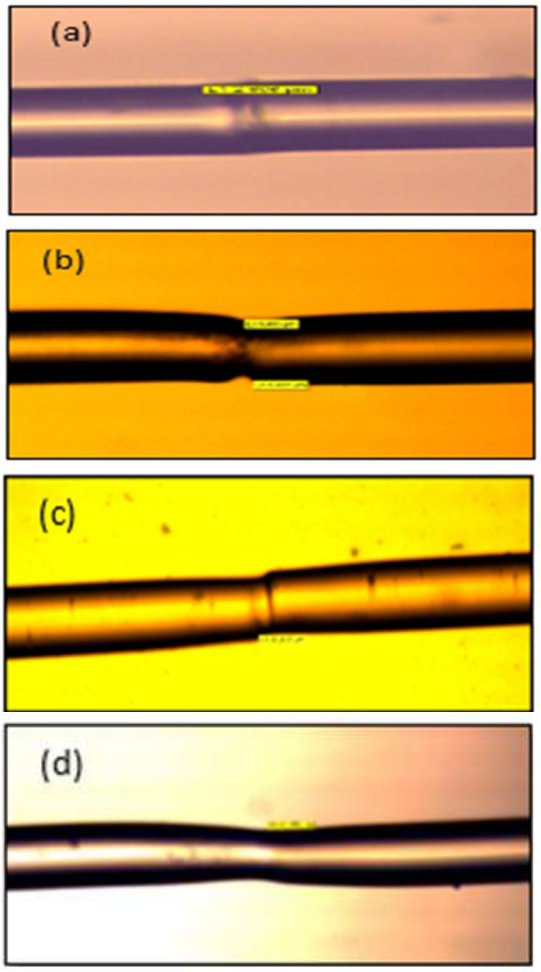

Fig.3: A microscope images for different offset distances, (a) offset for 2.6 µm, (b) offset for 6.4 µm, (c) offset for 12.1 µm, (d) offset for 18.3 µm.

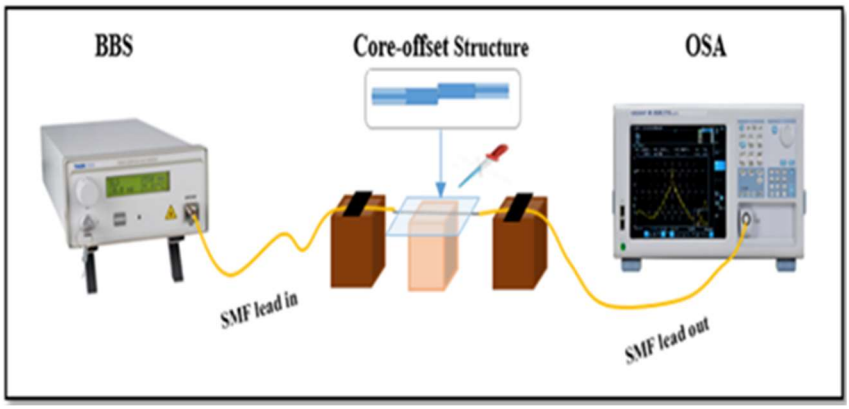

Fig.4: Sensor setup system.

The sensor setup system is shown in Figure 4. The structure configuration consisted of two SMFs lead in /lead out, and with SMFs lead in auto-spliced first section of CF (the coreless fiber is a special type of multimode fiber with uniform refractive index 1.444) (Thorlabs), a second symmetric section of CF that spliced with SMFs lead out and was spliced the two sections offset between them shows in figure 2 (a, b and c). The liquids pharmaceutical samples that were used for testing (Dististuled water, Nazordin droops, Allermine syrup, and Histadin syrup) have different RI (1.333, 1.335, 1.379, and 1.383) respectively. That is measured by (the ATAGO Refractometer). The sensor encompasses a broadband source (BBS) Thorlabs S5FC10055) with a wavelength range of (1400 nm to 1650 nm). To identify the response transmission spectra of the pharmaceuticals liquid sensor, BBS was joined to the SMF-CF-CF-SMF (SCCS) structure from the first section of SMF, and the second section of this structure was joined to an optical spectrum analyzer (OSA YOKOGAWA AQ6370C) display in Figure 4. A fusion splicer (Fujikura FSM-60S) with manual mode CF-CF offset splicing was used as shown in Figure 5.

Fig.5: CF-CF offset splicing.

3. Experiment results and dissection

In this work, the effect of length and offset distances on sensor sensitivity was investigated in this study were tested for each length (10mm, 15mm, 20mm, and 25mm) with different offsets (2.6 µm, 6.4 µm, 12.1 µm, 18.3 µm).

The sensitivity of the SCCS sensor for each offset was measured by wavelength shifting. The RI biosensor sensing performance was investigated as shown in Figure 6 (a, b, c, and d), Figure 7 (a, b, c and d), Figure 8 (a, b, c, and d), and Figure 9 (a, b, c and d) and Tables (1, 2, 3, and 4).

A. Experiment results and dissection for L=10 mm:

The first structure for L=10 mm with offset d=2.6 µm achieved higher sensitivity, which equaled 255.5 nm/RIU with wavelength shifts 23 nm, and the second structure with offset distance d=6.4 µm achieved sensitivity equaled 203.3 nm/RIU with wavelength shifts 18.3 nm while the third structure with offset distance 12.1 µm was achieved 218.8 nm/RIU with wavelength shifts 19.7 nm but it was unstable, finally the forth structure for 18.3 µm where the absence of dips this indicates that this offset with this length is not suitable.

Figure 6 displays how transmitted power varies with wavelength shifting for length L= 10 mm with each offset distance (a) d=2.6 µm (b) d= 6.4 µm, (c) d=12.1 µm, and (d) d=18.3 µm of similar sections of CF when the RI changes from 1 to 1.393.

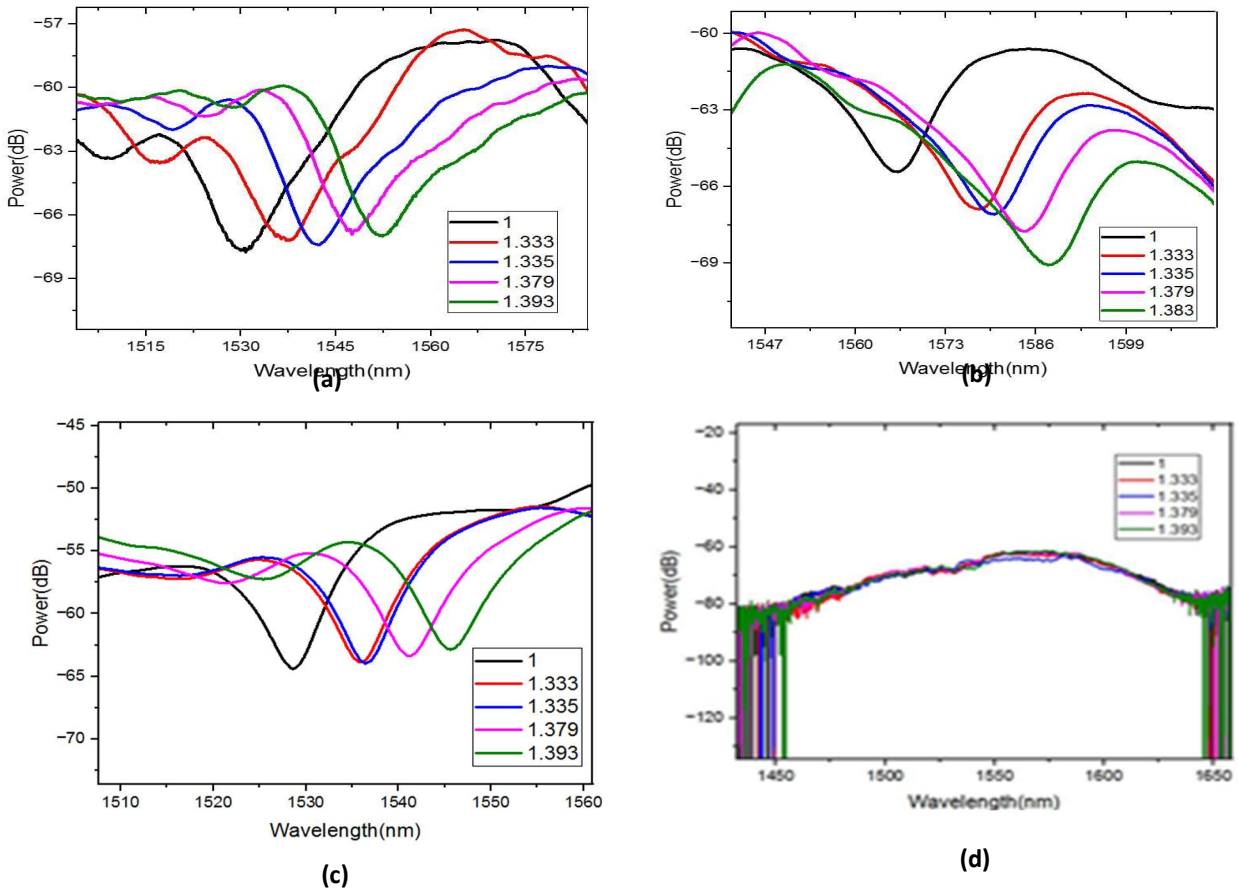

Fig.6: The Wavelength shifting at L=10 and variable d: (a) d=2.6 µm (b) d= 6.4 µm, (c) *d*=12.1 µm, and (d) *d*=18.3 µm.

Table 1. displays the wavelength shifts for L=10 mm at each offset distance.

Offset distance (µm)	2.6	6.4	12.1	18.3
Sensitivity (nm/RIU)	255.5	203.3	218.8	-
Wavelength shifts (nm)	23	18.29	19.7	-

B. Experiment results and dissection for L=15 mm

The first structure for this length with offset d=2.6 µm achieved a sensitivity equaled 222.7nm/RIU with wavelength shifts 20 nm, and the second structure for offset d=6.4 µm achieved a sensitivity equaled 227.7 nm/RIU with wavelength shifts 20.5 nm. In contrast, the third structure for offset 12.1 µm the absence of dips this indicates that this offset with this length is not suitable. Finally, the fourth structure for offset 18.3 µm achieved 231.1 nm/RIU with wavelength shifts 20.8 nm. Figure 7 displays the wavelength shifts for length L= 15 mm with each offset distance (a) d=2.6 µm (b) d= 6.4 µm, (c) *d*=12.1 µm, and (d) *d*=18.3 µm of similar sections of CF when the RI changes from 1 to 1.393.

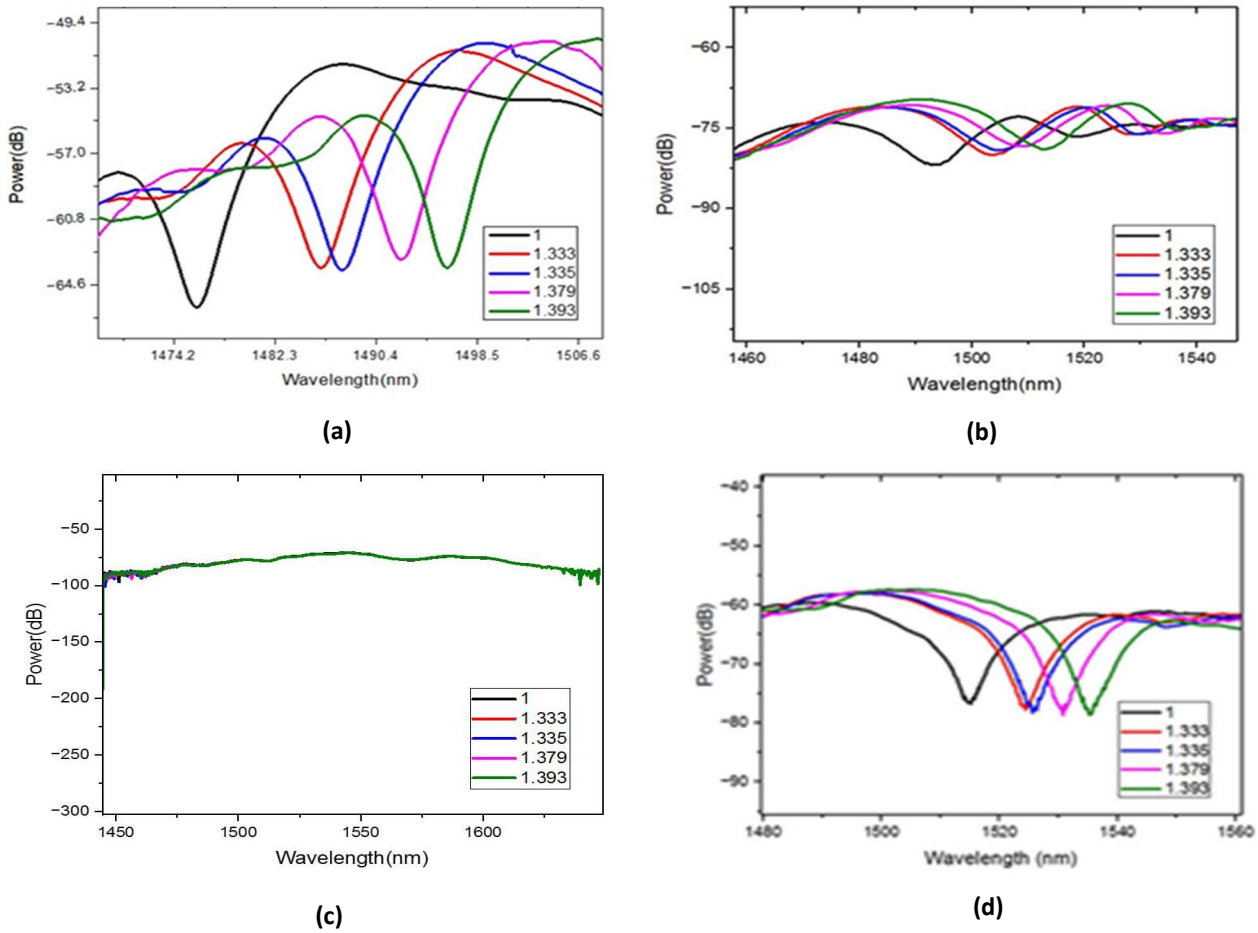

Fig.7: The Wavelength shifting at L=15 for offset distance d: (a) d=2.6 μm (b) d= 6.4 μm, (c) *d*=12.1 μm, and (d) *d*=18.3 μm.

Table 2. displays the wavelength shifts for L=15 mm at each offset distance.

Offset distance (μm)	2.6	6.4	12.1	18.3
Sensitivity (nm/RIU)	222.7	227.7	-	231.1
Wavelength shifts (nm)	20	20.5	-	20.8

C. Experiment results and dissection for L=20 mm

The first structure for this length with offset d=2.6 μm achieved a sensitivity equaled 212.7nm/RIU with wavelength shifts 19 nm, and the second structure for offset d=6.4 μm achieved a sensitivity equaled 214.4 nm/RIU with wavelength shifts 19.3 nm while the third structure for offset 12.1 μm the absence of dips this indicates that this offset with this length is not suitable, finally the forth structure for offset 18.3 μm achieved 231.1 nm/RIU with wavelength shifts 20.8 nm. Figure 8 displays the wavelength shifts for length L= 20 mm with each offset distance (a) d=2.6 μm (b) d= 6.4 μm, (c) *d*=12.1 μm, and (d) *d*=18.3 μm of similar sections of CF when the RI changes from 1 to 1.393.

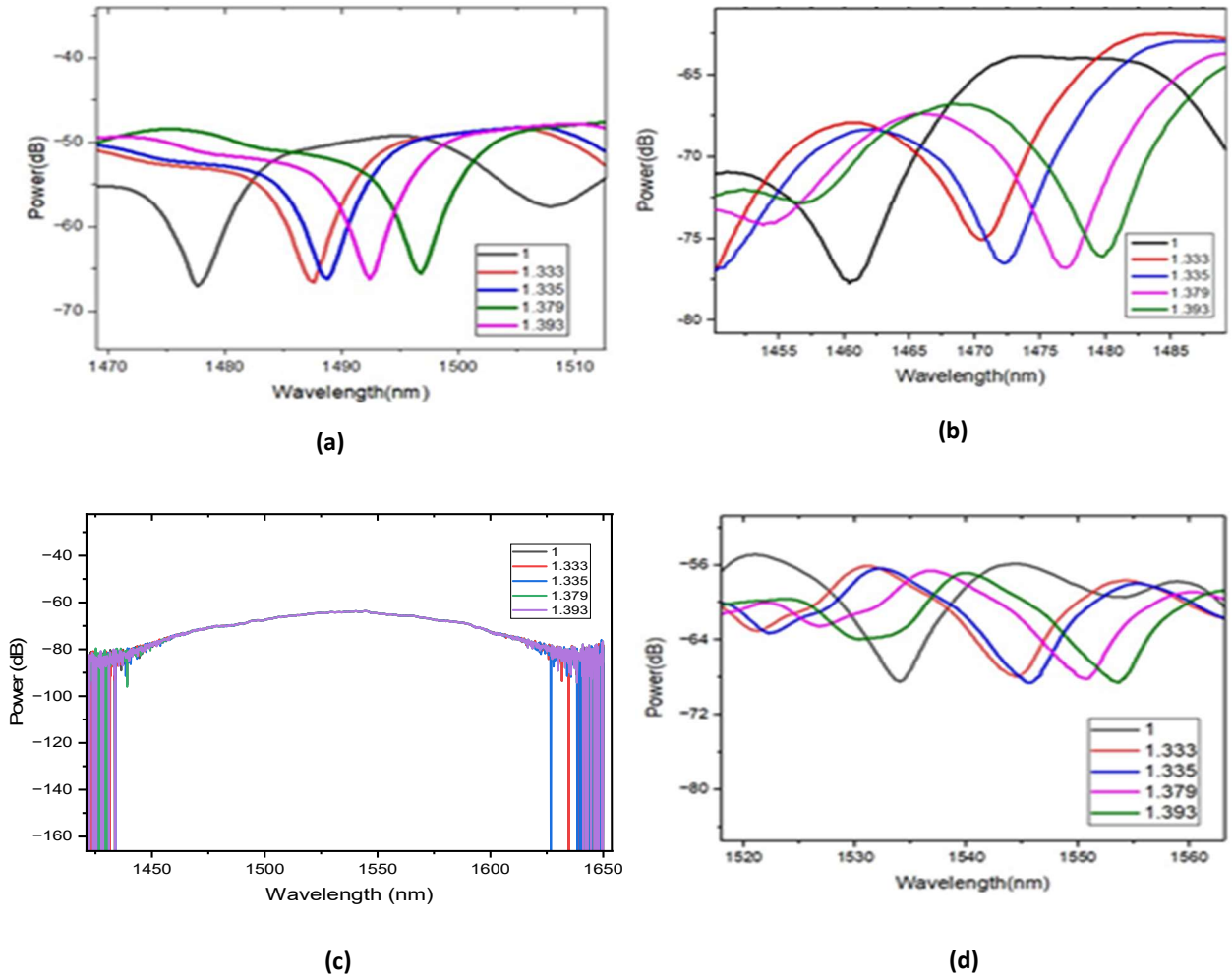

Fig. 8. The Wavelength shifting at L=20 for offset distance d: (a) d=2.6 μm (b) d= 6.4 μm, (c) *d*=12.1 μm, and (d) *d*=18.3 μm.

Table 3. displays the wavelength shifts for L=20 mm at each offset distance.

Offset distance (μm)	2.6	6.4	12.1	18.3
Sensitivity (nm/RIU)	212.7	214.4	-	227.3
Wavelength shifts (nm)	19	19.3	-	20.4

E. Experiment results and dissection for L=20 mm

The first structure for this length with offset d=2.6 μm achieved a sensitivity equaled 197.3 nm/RIU with wavelength shifts 17.8 nm, and the second structure for offset d=6.4 μm achieved a sensitivity equaled 190.4 nm/RIU with wavelength shifts 17.2 nm while the third structure for offset 12.1 μm achieved 220 nm/RIU with wavelength shifts 19.8 nm finally for offset18.3 μm the absence of dips this indicates that this offset with this length is not suitable, finally the forth structure for offset. Figure 9 displays the wavelength shifts for length L= 25 mm with each offset distance (a) d=2.6 μm (b) d= 6.4 μm, (c) *d*=12.1 μm, and (d) *d*=18.3 μm of similar sections of CF when the RI changes from 1 to 1.393.

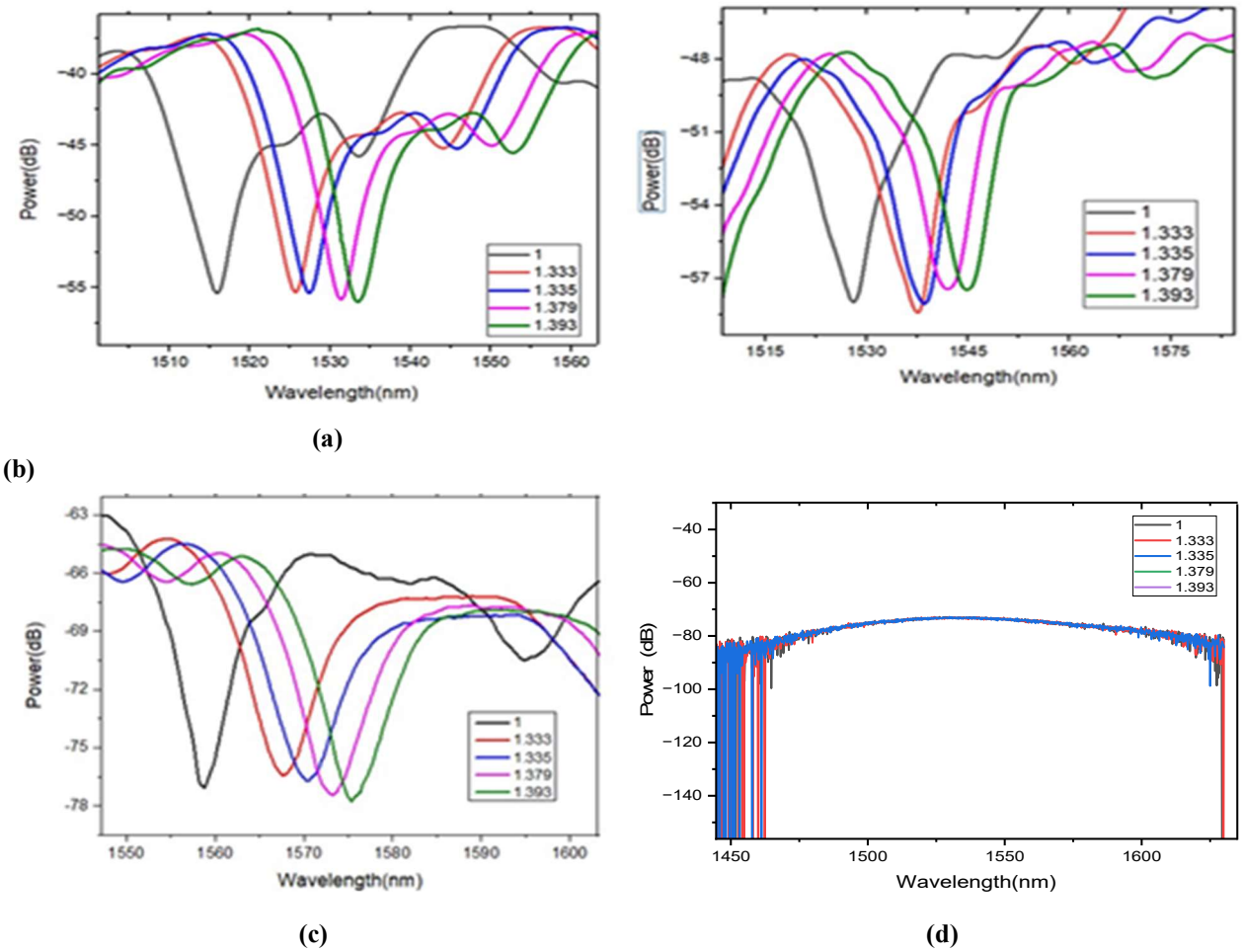

Fig.9: The Wavelength shifting at L=25 for offset distance d: (a) d=2.6 µm (b) d= 6.4 µm, (c) *d*=12.1 µm, and (d) *d*=18.3 µm.

Table 4. displays the wavelength shifts for L=25 mm at each offset distance.

Offset distance (µm)	2.6	6.4	12.1	18.3
Sensitivity (nm/RIU)	197.3	190.4	220	-
Wavelength shifts (nm)	17.8	17.2	19.8	-

We observed from this structure that sensitivity varied with length. The sensitivity increases as the length of the similar CF segments decreases. The wavelength shifts towards the long wavelength (red shift) when increasing the RI of samples. It is evident from the study of offset distance that the optimal offset at 2.6 µm with a length of CF-CF 10 mm. The reason for the high sensitivity of this new shape sensor is caused more evanescent waves could interact where there was more high order mode can be interference at three splicing areas when the refractive index was increased from 1 to 1.393. It has been proved that the offset and length of the CF - CF segments important parameters to increase the sensitivity of the sensor device. The refractive index biosensor synthesizes the merits of single mode coreless- coreless single mode (SMF-CF-CF-SMF) smart sensitive material with high flexibility in the design of accuracy in identifying and testing the construction of the drugs.

Table 5. Comparison between the sensitivities of this work and other RI sensors.

Sensor Structure	Offset Displacement	Refractive index range	Sensitivity (nm/ RIU)	Reference
Core offset FBG-SMF-SMF	8.1 µm	1.3232 to 1.3520	13.7592 nm/RI	[25]
SMF-peanut shape-SMF- core-off section-SMF	12 µm	1.333-1.373	-72.4	[26]
core offset SMF - SMF- SMF with tapered micrometers	7.5 µm	1.33 to 1.347.	16485 nm/RIU	[27]
SMF Taper-core-offset section AFMZI	6 µm	-	59.2	[28]
S and U-shapes study the effect of shape offset sensor	12.268 µm	1.33 to 1.38	98.786nm/RIU	[39]
SMF-CF-CF-SMF offset effect	2.6 µm	1 to 1.393	255.5 nm/RIU	In this study

4. Conclusions

In this work, a Refractive index biosensor based on the offset technique of coreless fiber was fabricated by the fusion splicer. The sensing part was composed of a similar section of CF that was spliced by the offset technique. The wavelength shifts of the sensor with different offset displacements and lengths were investigated. The experimental results showed that the sensitivity increased as the length of similar CF decreased, and when the offset displacement was 2.6 µm, and the length of a similar section of CF-CF was 10 mm, the RI sensitivity of 255.5 nm/RIU was obtained within the RI range from 1 to 1.393. The sensor exhibits the advantages of simple structure, high sensitivity, small size, low cost, and easy fabricating.

References

[1] A. Urrutia, K. Bojan, L. Marques, K. Mullaney, J. Goicoechea, S. James & S. Korposh. Novel highly sensitive protein sensors based on tapered optical fibers modified with Au-based nanocoatings. Journal of Sensors, 2016, 2016.
[2] Wang, B. T., & Wang, Q. (2018). An interferometric optical fiber biosensor with high sensitivity for IgG/anti-IgG immunosensing. Optics Communications, 426, 388-394.
[3] Damborsky, P.; Svitel, J.; Katrlik, J. Optical biosensors. Essays Biochem. 2016, 60, 91–100. [CrossRef] [PubMed
[4] Nikhil Bhalla, Pawan Jolly, Nello Formisano, and Pedro Estrela ‘’Introduction to biosensors‘’ Essays Biochem. 2016 Jun 30; 60(1): 1–8.
[5] Regatos, D. Biosensores ópticos de alta sensibilidad basados en técnicas de modulación plasmónica; Universidad de Santiago de Compostela: Barcelona, Spain, 2012.
[6] Lu, P.; Men, L.; Sooley, K.; Chen, Q. Tapered fiber Mach-Zehnder interferometer for simultaneous measurement of refractive index and temperature. Appl. Phys. Lett. 2009, 94, 131110.

[7] Li, B.; Jiang, L.; Wang, S.; Zhou, L.; Xiao, H.; Tsai, H.-L. Ultra-abrupt tapered Mach-Zehnder interferometer sensor. Sensors 2011, 11, 5729–5739.
[8] Li, L.; Li, X.; Xie, Z.; Liao, Z.; Tu, F.; Liu, D. Simultaneous measurement of refractive index and temperature using thinned fiber based Mach-Zehnder interferometer. Opt. Commun. 2012, 285, 3945–3949.
[9] Allsop, T.; Reeves, R.; Webb, D.J.; Bennion, I. A high-sensitivity refractometer based upon a long-period grating Mach-Zehnder interferometer. Rev. Sci. Instrum. 2002, 73, 1702–1705.
[10] Mata-Chavez, R.I.; Martines-Rios, A.; Torres-Gomez, I.; Selvas-Aguilar, R.; Estudillo-Ayala, J.M. Mach-Zehnder all Interferometer using two in-serie fattened gratings. Opt. Rev. 2008, 15, 230–235.
[11] Villatoro, J.; Finazzi, V.; Minkovich, V.P.; Pruneri, V.; Badenes, G.A. Temperature insensitive photonic crystal fiber interferometer for absolute strain sensing. Appl. Phys. Lett. 2007, 91, 091109.
[12] Wang, J.-N.; Tang, J.-L. Photonic crystal fiber Mach-Zehnder all Interferometer for refractive index sensing. Sensors 2012, 12, 2983–2995.
[13] Hu, L.M.; Chan, C.C.; Dong, X.Y.; Wang, Y.P.; Zu, P.; Wong, W.C.; Qian, W.W.; Li, T. Photonic crystal fiber strain sensor based on modified Mach-Zehnder interferometer. IEEE Photon. J. 2012, 4, 114–118.
[14] Sierra-Hernandez, J.M.; Castillo-Guzman, A.; Selvas-Aguilar, R.; Vargas-Rodriguez, E.; Gallegos-Arellano, E.; Guzman-Chavez, A.D.; Estudillo-Ayala, J.M.; Jauregui-Vazquez, D.; Rojas-Laguna, R. Torsion sensing setup based on three beam path Mach-Zehnder interferometer. Microw. Opt. Technol. Lett. 2015, 57, 1857–1860.
[15] Dong, X., Zeng, L., Chu, D., & Sun, X. (2022). Highly sensitive refractive index sensing based on a novel Mach-Zehnder interferometer with TCF-PCF composite structure. Infrared Physics & Technology, 123, 104134.
[16] Huerta-Mascotte, E., Sierra-Hernandez, J. M., Mata-Chavez, R. I., Jauregui-Vazquez, D., Castillo-Guzman, A., Estudillo-Ayala, J. M., ... & Rojas-Laguna, R. (2016). A core-offset Mach Zehnder interferometer based on a non-zero dispersion-shifted fiber and its torsion sensing application. Sensors, 16(6), 856.
[17] X. Yu, X. Chen, D. Bu, J. Zhang, S. Liu, In-fiber modal interferometer for simultaneous measurement of refractive index and temperature, IEEE Photon.Technol. Lett. 28 (2016) 189–192.
[18] Y. Zhao, X.-G. Li, L. Cai, A highly sensitive Mach-Zehnder interferometric refractive index sensor based on core-offset single mode fiber, Sens. Actuat. A: Phys. 223 (2015) 119–124.
[19] D.W. Duan, Y.J. Rao, L.C. Xu, T. Zhu, D. Wu, J. Yao, In-fiber Mach-Zehnder interferometer formed by large lateral offset fusion splicing for gases refractive index measurement with high sensitivity, Sens. Actuat. B: Chem. 160 (2011)1198–1202.
[20] D.W. Duan, Y.J. Rao, L.C. Xu, T. Zhu, D. Wu, J. Yao, In-fiber Mach-Zehnder interferometer formed by large lateral offset fusion splicing for gases refractive index measurement with high sensitivity, Sens. Actuat. B: Chem. 160 (2011) 1198–1202.
[21] Zhao, Y., Li, X. G., & Cai, L. (2015). A highly sensitive Mach–Zehnder interferometric refractive index sensor based on core-offset single-mode fiber. Sensors and Actuators A: Physical, 223, 119-124.
[22] Bahrain, N. F., Azmi, A. I., Abdullah, A. S., & Noor, M. Y. M. (2018).” Refractive index sensor based on lateral-offset of coreless silica interferometer”. Optics & Laser Technology, 99, 396-401.
[23] Aya R. Mejble, Hanan J. “S and U shape offset studying of the refractive index sensor based on coreless fiber”. Iraqi Journal of Laser, 2022, 21.2.
[24] Wahhab, A. A. A., Hammadi, Y. I., & Mansour, T. S. (2021). Design and Construct Nested Double Clad Multimode Fiber MZI (DC-MMF–NMZI) for Pregnancy Test. Journal of Mechanical Engineering Research and Developments, 44(10), 12-22.
[25] Zhang, Y. N., Sun, Y., Cai, L., Gao, Y., & Cai, Y. (2020). Optical fiber sensors for measurement of heavy metal ion concentration: A review. Measurement, 158, 107742.
[26] YAO, Qiqi, et al. Simultaneous measurement of refractive index and temperature based on a core-offset Mach–Zehnder interferometer combined with a fiber Bragg grating. Sensors and Actuators A: Physical, 2014, 209: 73-77.
[27] ZHOU, Yanfei; LIU, Yuan; ZHENG, Jie. An inline fiber Mach-Zehnder interferometer based on core offset and peanut shape for refractive index sensing. In: Optical Metrology and Inspection for Industrial Applications IX. SPIE, 2022. p. 396-403.
[28] LIAO, Yun-Cheng, et al. Ultrasensitive Microfiber Refractive Index Sensor Based on Mach-Zehnder Interference of Core Offset Structure. In: 2019 18th International Conference on Optical Communications and Networks (ICOCN). IEEE, 2019. p. 1-3.
[29] Aya R. Mejble* Hanan J. Taher. (2022). “ S and U shape offset studying of the refractive index sensor based on coreless fiber”. Iraqi Journal of Laser, 21(2), 33-40.

مستشعر معامل الانكسار الحيوي المعتمد على تقنية الأوفست للألياف عديمة النواة

سراء جمال إبراهيم* ، حنان جعفر طاهر

معهد الليزر للدراسات العليا، جامعة بغداد، بغداد، العراق

*البريد الالكتروني للباحث: saraa.najm2101m@ilps.uobaghdad.edu.iq

الخلاصة: اقترحت هذه الورقة بنية مستشعر حيوي باستخدام تقنية الإزاحة بين قطعتين متشابهتين من الألياف عديمة النواة (CF) مقسمة بين ليفين أحاديي الوضع لقياس حساسية معامل الانكسار للمستحضرات الصيدلانية السائلة. حيث تمت تجربة أطوال مختلفة لمقاطع CF لـ 10 ملم و15 ملم و20 ملم و25 ملم مع إزاحات مختلفة لـ 2.6 ميكرومتر و6.4 ميكرومتر و18.3 ميكرومتر لمقاطع CF المتناظرة. عند اختبار مؤشرات انكسار مختلفة (1، 1.333، 1.337، 1.369، 1.393) للمستحضرات الصيدلانية السائلة، يزداد الطول الموجي مع زيادة مؤشرات الانكسار، وتزداد الحساسية مع تقليل الطول أو الإزاحة. حيث تم تحقيق أعلى حساسية مع اصغر حجم للمتحسس هي 255.5 نانومتر/وحدة RIU، وهو ما يتوافق مع أعلى معامل انكسار قدره 1.393 لدواء شراب الهستادين، والذي تم الحصول عليه باستخدام الطول والإزاحة الأمثل. يتمتع هذا المستشعر الصغير بالقدرة على اكتشاف مؤشرات انكسار مختلفة للمواد الكيميائية والكيميائية الحيوية. يتمتع جهاز الاستشعار البيولوجي المقترح، ببنيته البسيطة وقدرات الاستشعار الخطية المحتملة، بالقدرة على التطور ليصبح أداة تنافسية وقابلة للتكيف لتحديد السوائل باستخدام معامل الانكسار. تشمل مزايا المستشعر المقترح الحساسية العالية والقدرة على التكيف، مما يتيح إجراء قياسات أسرع في الوقت الفعلي، وسهولة التصنيع والتشغيل، والحجم الصغير، والتصميم خفيف الوزن، والتكلفة المنخفضة.